Characterization of T Wave Amplitude, Duration and Morphology Changes During Hemodialysis: Relationship With Serum Electrolyte Levels and Heart Rate

Hassaan A. Bukhari ©, Flavio Palmieri ©, Julia Ramírez ©, Pablo Laguna ©, *Fellow, IEEE*,
José Esteban Ruiz, Dina Ferreira, Mark Potse ©, Carlos Sánchez ©, and Esther Pueyo ©

Abstract—Objective: **Chronic kidney disease affects more than 10% of the world population. Changes in serum ion concentrations increase the risk for ventricular arrhythmias and sudden cardiac death, particularly in end-stage renal disease (ESRD) patients. We characterized how T wave amplitude, duration and morphology descriptors change with variations in serum levels of potassium and calcium and in heart rate, both in ESRD patients and in simulated ventricular fibers. *Methods:* Electrocardiogram (ECG) recordings from twenty ESRD patients undergoing hemodialysis (HD) and pseudo-ECGs (pECGs) calculated from twenty-two simulated ventricular fibers at varying transmural heterogeneity levels were processed to quantify T wave width (T_{w}), T wave slope-to-amplitude ratio ($T_{\mathrm{S/A}}$) and four indices of T wave morphological variability based on time warping (d_{w}, $d_{\mathrm{w}}^{\mathrm{NL}}$, d_{a} and $d_{\mathrm{a}}^{\mathrm{NL}}$). Serum potassium and calcium levels and heart rate were measured along HD. *Results:* $d_{\mathrm{a}}^{\mathrm{NL}}$ was the marker most strongly correlated with serum potassium, d_{w} with calcium and d_{a} with heart rate, after correction for covariates. Median values of partial correlation coefficients were 0.75, −0.74 and −0.90, respectively. For all analyzed T wave descriptors, high inter-patient variability was observed in the pattern of such relationships. This variability, accentuated during the first HD time points, was reproduced in the simulations and shown to be influenced by differences in transmural heterogeneity. *Conclusion:* Changes in serum potassium and calcium levels and in heart rate strongly affect T wave descriptors, particularly those quantifying morphological variability. *Significance:* ECG markers have the potential to be used for monitoring serum ion concentrations in ESRD patients.**

***Index Terms*—Calcium, heart rate, hemodialysis, potassium, time warping, transmural heterogeneity, T wave morphology, ECG, *in silico* modeling.**

Hassaan A. Bukhari is with the BSICoS group, I3A Institute, University of Zaragoza, IIS Aragón, Zaragoza, Spain and with the CIBER en Bioingeniería, Biomateriales y Nanomedicina (CIBER-BBN), Spain and with the Carmen team, Inria Bordeaux – Sud-Ouest, Talence 33405, France, and also with the Univ. Bordeaux, IMB, UMR 5251, Talence (e-mail: hassaanahmed01@unizar.es).

Flavio Palmieri is with the CIBER en Bioingeniería, Biomateriales y Nanomedicina (CIBER-BBN) and also with the Centre de Recerca en Enginyeria Biomèdica, Universitat Politècnica de Catalunya.

Julia Ramírez is with the William Harvey Research Institute, Queen Mary University of London.

Pablo Laguna and Esther Pueyo are with the BSICoS group, I3A Institute, University of Zaragoza, and also with the CIBER en Bioingeniería, Biomateriales y Nanomedicina (CIBER-BBN).

José Esteban Ruiz is with the Nephrology Department, Hospital Clínico Universitario Lozano Blesa.

Dina Ferreira is with the Laboratorios Rubio Castellbisbal, Barcelona.

Mark Potse is with the Carmen team, Inria Bordeaux – Sud-Ouest, and also with the Univ. Bordeaux, IMB.

Carlos Sánchez is with the BSICoS group, I3A Institute, University of Zaragoza, IIS Aragón, Zaragoza, Spain and with the CIBER en Bioingeniería, Biomateriales y Nanomedicina (CIBER-BBN), and also with the Defence University Centre, General Military Academy, Zaragoza, Spain.

Digital Object Identifier 10.1109/TBME.2020.3043844

I. Introduction

C HRONIC kidney disease represents a global health burden, with an estimated 10% of the population being affected. All stages of this disease, but particularly the late ones, are associated with increased mortality and decreased quality of life [1]. Hemodialysis (HD) is a common treatment for patients in whom the disease has progressed to end-stage renal disease (ESRD). The main causes of death among ESRD patients undergoing HD are cardiovascular diseases, all together accounting for 43% of mortality [2]. Many of these deaths are due to ventricular arrhythmias and sudden cardiac death [3].

ESRD patients show impaired ability to maintain electrolyte balance in the bloodstream. Serum potassium ($[\mathrm{K}^+]$) and calcium ($[\mathrm{Ca}^{2+}]$) levels outside normal ranges, in the form of hypo- or hyperkalemia and hypo- or hypercalcemia, are known to increase the risk for life-threatening arrhythmias [4]–[7]. HD can even enhance arrhythmic risk due to changes in volume and electrolyte concentrations associated with the intermittent nature of the treatment [8].

$[\mathrm{K}^+]$ and $[\mathrm{Ca}^{2+}]$ variations are known to influence the electrocardiogram (ECG) [7], [9]–[11]. In a recent large-scale study on unselected individuals, shorter QT intervals were associated with higher $[\mathrm{K}^+]$ and $[\mathrm{Ca}^{2+}]$ [7]. In [12], a single-lead ECG

estimator of $[K^+]$ based on the ratio of the T wave downward slope and the square root of T wave amplitude was proposed and validated in 19 HD patients. On a similar basis, a multi-lead ECG estimator of $[K^+]$ based on the ratio of the downward slope and amplitude of the T wave was proposed and validated in 45 HD patients [13]–[15]. Computational modeling has also been used to assess the effects of changes in $[K^+]$, $[Ca^{2+}]$ and sodium ($[Na^+]$) concentrations on simulated action potentials (APs) and ECGs [16]–[18]. An inverse relationship between $[K^+]$ and $[Ca^{2+}]$, on the one hand, and simulated QT and RT intervals, on the other, was reported, with negligible effects of $[Na^+]$ changes on those intervals. These *in silico* studies were, however, based on a single ventricular model not accounting for potential inter-individual variability.

Although the mentioned studies suggest that it is possible to monitor changes in $[K^+]$ and $[Ca^{2+}]$ based on ECG analysis, further investigation is needed to demonstrate the feasibility of such approach. On the one hand, most of the proposed markers rely on only one specific ECG interval duration or wave amplitude that may present large variations not necessarily associated with electrolyte levels. Also, some of the proposed ECG markers cannot always be robustly measured due to difficulties in the delineation of low-amplitude waves, which could hinder their use for ambulatory monitoring. Importantly, the physiological underpinnings of changes in the proposed ECG markers in association with electrolyte variations have not been well established. We hypothesize that markers accounting for the whole T wave morphology can more robustly characterize repolarization changes associated with different $[K^+]$ and $[Ca^{2+}]$ levels and, thus, be better suited for non-invasive electrolyte estimation. Additionally, simulation of ECGs from a set of human ventricular tissue models representing potential inter-patient differences can help in the interpretation of the obtained results.

The aim of this work is to characterize changes in T wave amplitude, duration and morphology, the latter both in the time and amplitude domains, during HD in relation to $[K^+]$ and $[Ca^{2+}]$ variations. Since heart rate (HR) may play a role in those relationships, its effects are also assessed. To uncover potential cellular mechanisms underlying differential T wave responses to variations in $[K^+]$, $[Ca^{2+}]$ and RR (inverse of instantaneous HR), a set of transmural ventricular fibers covering a wide range of cellular heterogeneities is simulated and pseudo-ECGs (pECGs) are computed. A sensitivity analysis is performed to investigate the extent to which different proportions of endocardial, midmyocardial and epicardial cells contribute to explain inter-individual differences in T wave amplitude, time and morphology, particularly for $[K^+]$ and $[Ca^{2+}]$ values outside normal ranges. Preliminary results were presented as a conference contribution [19].

II. MATERIALS AND METHODS

A. Study Population and Data Analysis

The study population included 20 ESRD patients from Hospital Clínico Universitario de Zaragoza (HCUZ). 48-hour 12-lead ECGs were acquired at a sampling frequency of 1 kHz with an amplitude resolution of 3.75 μV (H12+, Mortara Instruments,
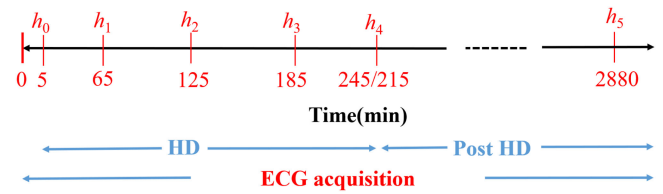

Fig. 1. Diagram of the study protocol. h_0 to h_5 are the time points (in minutes) for blood sample extraction.

TABLE I
CHARACTERISTICS OF THE ESRD STUDY POPULATION. VALUES ARE EXPRESSED AS NUMBER (%) FOR CATEGORICAL VARIABLES AND MEDIAN (INTERQUARTILE RANGE) FOR CONTINUOUS VARIABLES

Characteristics	Quantity
Age [years]	72 (10)
Gender [male/female]	14/6
Electrolyte concentrations	
$[K^+]$ [Pre HD] (mM)	5.36 (1.69)
$[K^+]$ [End HD] (mM)	3.25 (0.63)
$[Ca^{2+}]$ [Pre HD] (mM)	2.15 (0.17)
$[Ca^{2+}]$ [End HD] (mM)	2.35 (0.17)
	#Patients (%)
HD session duration	
240 min	17 (85%)
210 min	3 (15%)
Dialysate composition	
Potassium (1.5 mEq/L)	17 (85%)
Potassium (variable mEq/L)	3 (15%)
Calcium (1.5 mEq/L)	6 (30%)
Calcium (1.25 mEq/L)	14 (70%)

Milwaukee, WI, USA). The acquisition started 5 minutes before the onset of HD treatment and lasted for 48 hours (Fig. 1, bottom blue line). Five blood samples were taken and analyzed for $[K^+]$ and $[Ca^{2+}]$ during the HD session: the first one at the HD onset and the next three samples every hour during the HD session (Fig. 1, h_0 to h_3 in red). The $5th$ blood sample was collected at the end of the HD (h_4, at minute 215 or 245, depending on the patient). A $6th$ blood sample, h_5, was taken after 48 hours, immediately before the next HD session, but was not analyzed as part of this work. The study protocol was approved by the ethical committee (CEICA ref. PI18/003) and all patients signed the informed consent form. Table I shows the population characteristics.

B. ECG Pre-Processing

Pre-processing of ECG signals from ESRD patients included band-pass filtering (0.5–40 Hz) to remove baseline wander as well as muscular and powerline noise. A wavelet-based single-lead delineation method was used for QRS detection and wave delineation of each of the twelve leads [20].

Principal component (PC) analysis was spatially applied to the T waves of the eight independent leads [21] to enhance the T wave energy. The coefficients defining the PC transformation were obtained from the eigenvectors of the 8×8 inter-lead auto-correlation matrix estimated by including all segmented T waves within a 10-minute window at the end of the HD session, as this is the time when the patient was discharged from hospital with

restored serum ion levels, thus being an acceptable reference for ambulatory monitoring. The first PC computed by projecting the ECG recording was used for subsequent ECG analysis, as it is the transformed lead where the T waves have maximal energy, thus allowing better morphological characterization.

The T waves in the first PC were delineated using the single-lead delineation algorithm described in [20]. The onset, peak and end of the T waves were determined [20] and used for subsequent computation of T wave markers.

C. Time, Amplitude and Morphology-Based T wave Descriptors

1) Time and Amplitude T Wave Markers: Time- and amplitude-based T wave descriptors were computed from mean warped T waves (MWTWs). To obtain a MWTW, which is an optimal representative average both in temporal and amplitude domains [22], two-minute ECG segments at the end of each HD hour were analyzed. A predominant T wave polarity was defined as the most frequent in the analyzed two-minute window. T waves having the predominant polarity were aligned with respect to their gravity center and used to compute an initial MWTW [22]. After removing outliers from the selected T waves, the remaining T waves presenting strong correlation (Spearman's correlation coefficient > 0.98) with the previous initial MWTW were considered to compute the final MWTW.

The analyzed T wave descriptors, computed from MWTWs at time points h_0, h_1, h_2, h_3 and h_4 during HD, included:

- T_w, representing T wave width calculated from T wave onset to T wave end (expressed in ms) [20].
- $T_{S/A}$, representing the ratio between the maximal downward slope (in absolute value) and the amplitude of the T wave (expressed in 1/ms) [14], [15].

2) T wave Markers Based on Morphological Characteristics: Morphology-based T wave descriptors were computed using the time-warping methodology described previously [22]. For the patients' ECGs, reference T waves were calculated from the MWTW at the end of the HD session.

The T wave for a given HD time point was expressed as $\mathbf{f}^s(\mathbf{t}^s) = [f^s(t^s(1)), \ldots, f^s(t^s(N_s))]^\top$ and the reference T wave as $\mathbf{f}^r(\mathbf{t}^r) = [f^r(t^r(1)), \ldots, f^r(t^r(N_r))]^\top$, where $\mathbf{t}^r = [t^r(1), \ldots, t^r(N_r)]^\top$, $\mathbf{t}^s = [t^s(1), \ldots, t^s(N_s)]^\top$ and N_r and N_s are the total durations of $\mathbf{t}^r$ and $\mathbf{t}^s$, which are the uniformly sampled time vectors corresponding to the T waves $\mathbf{f}^s$ and $\mathbf{f}^r$, respectively. Fig. 2 (a) shows $\mathbf{f}^r$ and $\mathbf{f}^s$, with their respective time domains, $\mathbf{t}^r$ and $\mathbf{t}^s$. Let $\gamma(\mathbf{t}^r)$ be the warping function that relates $\mathbf{t}^r$ and $\mathbf{t}^s$, such that $\mathbf{f}^s(\gamma(\mathbf{t}^r))$ denotes the time-domain warping of $\mathbf{f}^s(\mathbf{t}^s)$ using $\gamma(\mathbf{t}^r)$. The square-root slope function (SRSF) transformation was used to find the optimal warping function by warping the SRSFs of the original T waves [22]. This transformation is defined as:

$$\mathbf{q}_f(\mathbf{t}) = \text{sign}(\dot{\mathbf{f}}(\mathbf{t}))|\dot{\mathbf{f}}(\mathbf{t})|^{\frac{1}{2}}. \qquad (1)$$

The optimal warping function was determined as the one minimizing the SRSF amplitude difference:

$$\gamma^*(\mathbf{t}^r) = \underset{\gamma(\mathbf{t}^r)}{\arg\min}\left(\left\|\mathbf{q}_{f^r}(\mathbf{t}^r) - \mathbf{q}_{f^s}(\gamma(\mathbf{t}^r))\sqrt{\dot{\gamma}(\mathbf{t}^r)}\right\|\right). \qquad (2)$$
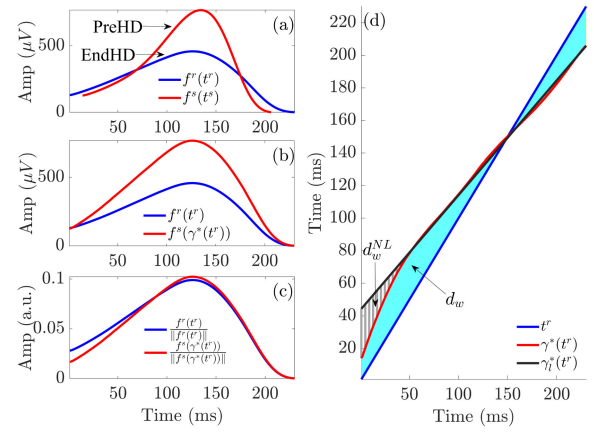

Fig. 2. Linear and non-linear time warping for a patient. Panel (a) shows reference (blue) and investigated (red) T waves obtained from an ECG segment during HD. Panel (b) shows the warped T waves, which have the same duration while keeping the original amplitude. Panel (c) depicts the warped T waves after normalization by their L2-norms. The area (cyan region) between both T waves in panel (d) represents d_w, which quantifies the total amount of warping. The black solid line is the linear regression function $\gamma_l^*(t^r)$ best fitted to $\gamma^*(t^r)$. The marker d_w^{NL} quantifies the non-linear warping by computing the area of the dashed grey region between $\gamma^*(t^r)$ and $\gamma_l^*(t^r)$.

A dynamic programming algorithm was used to obtain the function $\gamma^*(\mathbf{t}^r)$ that optimally warps $\mathbf{f}^r(\mathbf{t}^r)$ into $\mathbf{f}^s(\mathbf{t}^s)$. This function is shown in Fig. 2 (d). The warped T wave, $\mathbf{f}^s(\gamma^*(\mathbf{t}^r))$, is shown in Fig. 2 (b), together with the reference T wave, $\mathbf{f}^r(\mathbf{t}^r)$.

The descriptor d_w, shown in Fig. 2 (d), was used to quantify the level of warping required to optimally align the T waves $\mathbf{f}^s(\mathbf{t}^s)$ and $\mathbf{f}^r(\mathbf{t}^r)$:

$$d_w = \left(\frac{s_d}{|s_d|}\right)\frac{1}{N_r}\sum_{n=1}^{N_r}|\gamma^*(t^r(n)) - t^r(n)|, \qquad (3)$$

where $s_d = \sum_{n=1}^{N_r^u}(\gamma^*(t^r(n)) - t^r(n)) + \sum_{n=N_r^u+1}^{N_r}(t^r(n) - \gamma^*(t^r(n)))$ is used to account for the sign, with N_r^u denoting the number of samples in the T wave upslope.

The amplitude descriptor d_a was computed from the area contained between $\mathbf{f}^r(\mathbf{t}^r)$ and $\mathbf{f}^s(\gamma^*(\mathbf{t}^r))$ normalized by the L2-norm of $\mathbf{f}^r(\mathbf{t}^r)$, thus quantifying amplitude differences after time warping the two T waves:

$$d_a = \frac{s_a}{|s_a|}\frac{\|\mathbf{f}^s(\gamma^*(\mathbf{t}^r)) - \mathbf{f}^r(\mathbf{t}^r)\|}{\|\mathbf{f}^r(\mathbf{t}^r)\|} \times 100, \qquad (4)$$

where $s_a = \sum_{n=1}^{N_r}(f^s(\gamma^*(t^r(n))) - f^r(t^r(n)))$ is used to account for the sign.

The warping parameter d_w has a positive sign if the analyzed T wave is globally widened during the warping procedure to fit the reference T wave, and a negative sign if the T wave is compressed. In the amplitude domain, d_a is positive if the warped T wave has larger amplitude than the reference T wave, and negative if the T wave has smaller amplitude.

The marker d_w incorporates information from the linear and non-linear warping required to fit the two T waves in the time

domain. The non-linear component of d_w can be quantified as:

$$d_w^{\mathrm{NL}} = \frac{1}{N_r} \sum_{n=1}^{N_r} |\gamma^*(t^r(n)) - \gamma_l^*(t^r(n))|, \qquad (5)$$

where $\gamma_l^*(t^r)$ (black line in Fig. 2 (d)) was derived by linearly fitting $\gamma^*(t^r)$ through the least absolute residual method.

The marker d_a^{NL} was defined by computing the L_2 norm of the difference between L_2-normalized versions of $\mathbf{f}^r(\mathbf{t}^r)$ and $\mathbf{f}^s(\gamma^*(\mathbf{t}^r))$:

$$d_a^{\mathrm{NL}} = \left\| \frac{\mathbf{f}^r(\mathbf{t}^r)}{\|\mathbf{f}^r(\mathbf{t}^r)\|} - \frac{\mathbf{f}^s(\gamma^*(\mathbf{t}^r))}{\|\mathbf{f}^s(\gamma^*(\mathbf{t}^r))\|} \right\| \times 100. \qquad (6)$$

The set of all morphology-based T wave markers analyzed in this study included:

- d_w, representing temporal variations in T wave morphology (expressed in ms),
- d_a, representing amplitude variations in T wave morphology (expressed as a %),
- d_w^{NL}, representing non-linear temporal variations in T wave morphology (expressed in ms),
- d_a^{NL}, representing non-linear amplitude variations in T wave morphology (expressed as a %).

D. Relationship Between T Wave Markers and $[\mathrm{K}^+]$, $[\mathrm{Ca}^{2+}]$ and HR Variations

To assess the effects of $[\mathrm{K}^+]$, $[\mathrm{Ca}^{2+}]$ and RR on each investigated T wave marker at different time points during HD, linear correlation analysis was performed [23], [24]. Let X represent $[\mathrm{K}^+]$, $[\mathrm{Ca}^{2+}]$ or RR and let Y be one of the markers T_w, $T_{\mathrm{S/A}}$, d_w, d_a, $d_\mathrm{w}^{\mathrm{NL}}$ and $d_\mathrm{a}^{\mathrm{NL}}$. The correlation coefficient between X and Y was then computed as:

$$\rho_{XY} = \frac{\sum (X - \bar{X})(Y - \bar{Y})}{\sqrt{\sum (X - \bar{X})^2 \cdot \sum (Y - \bar{Y})^2}}. \qquad (7)$$

where $\bar{X}$ and $\bar{Y}$ are the sample means.

To independently quantify the effects of $[\mathrm{K}^+]$, $[\mathrm{Ca}^{2+}]$ and RR on each T wave marker, linear partial correlation analysis was performed [25], [26]. The correlation coefficient after removing the effects of Z in both X and Y was calculated as:

$$\rho_{XY \cdot Z} = \frac{\rho_{XY} - \rho_{XZ}\rho_{ZY}}{\sqrt{(1 - \rho_{XZ}^2) \cdot (1 - \rho_{ZY}^2)}}. \qquad (8)$$

The correlation coefficient between X and Y after removing the effects of two variables Z_0 and Z_1 was calculated as:

$$\rho_{XY \cdot z_0 z_1} = \frac{\rho_{XY \cdot z_0} - (\rho_{Xz_1 \cdot z_0}) \cdot (\rho_{Yz_1 \cdot z_0})}{\sqrt{(1 - \rho_{Xz_1 \cdot z_0}^2) \cdot (1 - \rho_{Yz_1 \cdot z_0}^2)}}, \qquad (9)$$

where $\mathrm{Z}_0, \mathrm{Z}_1 \in \{[\mathrm{K}^+], [\mathrm{Ca}^{2+}], \mathrm{RR}\}$.

To test for significant differences in $[\mathrm{K}^+]$, $[\mathrm{Ca}^{2+}]$, RR, T_w, $T_{\mathrm{S/A}}$, d_w, d_a, $d_\mathrm{w}^{\mathrm{NL}}$ and $d_\mathrm{a}^{\mathrm{NL}}$ at different HD time points, Wilcoxon signed-rank tests were performed [27] and p-values (p) were computed. The use of a non-parametric statistical test was based on the lack of normality of the data distributions according to Shapiro-Wilk test.

Also, to test whether Pearson correlation between each T wave marker and $[\mathrm{K}^+]$, $[\mathrm{Ca}^{2+}]$ or RR was significantly different from 0 in mean over the population, Student's t-test was performed after converting the statistical distribution of ρ into a normal distribution by application of Fisher's z transform [28].

E. In Silico Population of Human Ventricular Fibers

Transmural electrical propagation from ventricular endocardium to epicardium was simulated using one-dimensional fibers of 1.65 cm in length [15], [29]. Cellular electrophysiology was represented by the human ventricular AP model proposed by Ten Tusscher and Panfilov [30]. To adequately represent the relationship between AP duration (APD) and $[\mathrm{Ca}^{2+}]$, the updates to the Ten Tusscher-Panfilov model published in [31] were incorporated.

Different proportions of endocardial, midmyocardial and epicardial cells were simulated in a total of 22 combinations with 10% variations in the proportion of each cell type: endocardial layer ranging from 10% to 50%, midmyocardial layer from 10% to 50% and epicardial layer from 20% to 80%. We used the notation Cuvw, where C stands for the word "case" and u, v and w denote the first digit of the proportions of endocardial, midmyocardial and epicardial cells, respectively (e.g. C334 represents the case with 30%, 30% and 40% of endocardial, midmyocardial and epicardial cells, respectively).

A train of 10 stimuli was applied to the first cell of each fiber with a basic cycle length of 1000 ms and amplitude equal to 1.5 times the diastolic threshold. The initial state for each simulation was pre-calculated from a single cell simulation, where the values of the model state variables after 1000 paced beats were considered as representative of the cell at steady state. To compute electrical propagation, a finite element-based software [32] was used with a time step of 0.01 ms and space discretization of 0.01 cm.

Unipolar pECGs were computed as described in previous studies [29] using the expression:

$$V_\mathrm{e}(x,' y,' z') = \epsilon \int \frac{\partial V(x,y,z)}{\partial x} \cdot \left(\frac{\partial}{\partial x} \left(\frac{1}{r(x,y,z)} \right) \right) \, dx, \qquad (10)$$

where ϵ is a constant proportional to the ratio of intracellular and extracellular conductivities, $V(x,y,z)$ is the transmembrane potential and $r(x,y,z)$ is the distance between each source point (x,y,z) in the 1D fiber and the virtual electrode $(x,' y,' z')$ located, in this study, 2 cm away from the epicardium in the fiber direction: $r(x,y,z) = ((x - x')^2 + (y - y')^2 + (z - z')^2)^{1/2}$, where $y = y'$ and $z = z'$ are constant.

F. Effects of $[\mathrm{K}^+]$, $[\mathrm{Ca}^{2+}]$ and HR Variations on Simulated T waves

To assess the extent of the contribution of each investigated factor, i.e. $[\mathrm{K}^+]$, $[\mathrm{Ca}^{2+}]$ and RR, to T wave characteristics, simulations were conducted for each ventricular fiber under varying values of those factors and the corresponding pECGs were computed. The range of simulated $[\mathrm{K}^+]$ values included the default level in the Ten Tusscher-Panfilov model, i.e. $[\mathrm{K}^+] = 5.4$ mM, as

well as other levels below and above it: $[\mathrm{K^+}] \in \{3, 4, 5.4, 6.2\}$ mM. In the case of $[\mathrm{Ca^{2+}}]$, the range of simulated values included the default level of 2 mM, and values around it: $[\mathrm{Ca^{2+}}] \in \{1.4, 2, 2.6, 3.2\}$ mM. For RR, the variations were in accordance to the range measured from the ECGs of the patients: $\mathrm{RR} \in \{0.6, 0.8, 1, 1.2\}$ s. In the following, the notation $\mathcal{F}\{[\mathrm{K^+}], [\mathrm{Ca^{2+}}], \mathrm{RR}\}$ is used to represent simulated cases with varying $[\mathrm{K^+}]$, $[\mathrm{Ca^{2+}}]$ and RR.

The last pECG beat of each simulated condition was delineated using the same delineation method mentioned above [20]. The time-, amplitude- and morphology-based T wave descriptors of section II-C were measured over those pECGs. For warping-based markers, reference T waves were calculated from the simulated beats generated for minimum $[\mathrm{K^+}]$ (3 mM) and maximum $[\mathrm{Ca^{2+}}]$ (3.2 mM) and RR (1.2 s), that is $\mathcal{F}\{3\,\mathrm{mM}; 3.2\,\mathrm{mM}; 1.2\,\mathrm{s}\}$.

G. Sensitivity Analysis for Assessment of Inter-Individual Variability

Sensitivity analysis was performed to assess how the proportion, a, of endocardial, midmyocardial and epicardial cell layers, c, modulated T wave morphology descriptors, Y, at different $[\mathrm{K^+}]$, $[\mathrm{Ca^{2+}}]$ or RR levels. For each T wave descriptor at each given concentration of $[\mathrm{K^+}]$ ($[\mathrm{Ca^{2+}}]$ or RR, respectively), the percentage of change ($D_{Y;c;a_i}$) and its sensitivity ($S_{Y;c;a1,a2}$) to changes in the proportion of cells of each ventricular layer were computed as follows [33]:

$$D_{Y;c;a_i} = \left(\frac{Y_{c;a_i} - Y_{C334}}{Y_{C334}} \right) \cdot 100, \quad i \in \{1, 2\} \tag{11}$$

$$S_{Y;c;a_1,a_2} = \frac{(D_{Y;c;a_2} - D_{Y;c;a_1})100}{a_2 - a_1} = \frac{(Y_{c;a_2} - Y_{c;a_1})100^2}{Y_{C334}(a_2 - a_1)}, \tag{12}$$

where $Y_{c;a}$ is the average value of the T wave marker Y from all possible combinations $\mathrm{C}uvw$ sharing a proportion a, at the c layer of endocardial, midmyocardial or epicardial cells, $c \in \{\mathrm{Endo, Mid, Epi}\}$, with respect to case C334, which was used as a reference [34]. The values of a_1 and a_2 were taken as the minimum and maximum proportions of cells in each layer, respectively: 10% and 50% for endocardial and midmyocardial cells, and 20% and 80% for epicardial cells.

Y_{C334} is the value of the T wave descriptor for reference case C334. Thus, $D_{Y;c;a_i}$ measures the mean percentage of change in the T wave marker Y when varying the proportion of cells in layer c to a percentage a_i, $i \in \{1, 2\}$, with respect to that in C334. $S_{Y;c;a_1,a_2}$ measures the sensitivity of Y when varying the proportion of cells in layer c from a_1 to a_2.

III. RESULTS

A. Characterization of T wave Changes During HD

Fig. 3, panels (a–f), presents the results for all the T wave markers during the HD session for the 20 analyzed patients, while panels (g-i) present the evolution of $[\mathrm{K^+}]$, $[\mathrm{Ca^{2+}}]$ and RR during the session. In all these panels, significant differences

between consecutive HD time points are indicated. The bottom panels illustrate variations in T waves for one patient during the session, with the reference T wave at the end of the HD session shown in blue and each investigated T wave shown in red. $[\mathrm{K^+}]$ and $[\mathrm{Ca^{2+}}]$ vary strongly during the session, whereas the RR interval varies much less.

A decreasing trend of $T_{\mathrm{S/A}}$, d_{w}, $d_{\mathrm{w}}^{\mathrm{NL}}$, d_{a} and $d_{\mathrm{a}}^{\mathrm{NL}}$ and an increasing trend of T_{w} during the HD session can be observed, with significantly different values along time. In the bottom panels, significant changes in the T wave morphology are seen to accompany the fluctuations of $[\mathrm{K^+}]$, $[\mathrm{Ca^{2+}}]$ and RR during the session. In the example shown in the bottom panels of Fig. 3 for a particular patient, tall and narrow peaked PCA-transformed T waves are observed at the start of the HD session (h_0) corresponding to maximal $[\mathrm{K^+}]$.

B. In Silico Assessment of T Wave Changes Due to $[\mathrm{K^+}]$ Variations

T wave markers computed from simulated pECGs at varying $[\mathrm{K^+}]$ are shown in Fig. 4. Panels (a-d) show the simulated APs along the 1-D fiber for the simulated case C154 and $\mathcal{F}\{[\mathrm{K^+}]; 2.0\,\mathrm{mM}; 1.0\,\mathrm{s}\}$ when $[\mathrm{K^+}]$ is varied from 6.2 mM to 3 mM. The range of simulated $[\mathrm{K^+}]$ values approximately corresponds to the maximum and minimum $[\mathrm{K^+}]$ range calculated from the patients' blood data. The corresponding changes in the simulated pECGs are shown in panels (e-h). It can be observed from the figure that a variation in $[\mathrm{K^+}]$ causes AP shortening or prolongation in endocardial, midmyocardial and epicardial cells and therefore shorter or longer QT intervals as well as variations in the width, amplitude and morphology of the T wave.

T wave markers computed from the simulated pECGs are presented in panels (i-n) for the different levels of $[\mathrm{K^+}]$. All T wave markers present clear variations with $[\mathrm{K^+}]$, reproducing a behavior observed in the patients (Fig. 3). A decreasing trend of d_{w} and $d_{\mathrm{a}}^{\mathrm{NL}}$ from the maximum to the minimum level of $[\mathrm{K^+}]$ was observed in all the simulated cases (panels j and n). Monotonic trends of T_{w}, $T_{\mathrm{S/A}}$, d_{a} and $d_{\mathrm{w}}^{\mathrm{NL}}$ were observed in most of the simulated cases (panels i, l, m and n).

The bottom panels in Fig. 4 illustrate variations in T waves for simulated fiber C154 from the maximum to the minimum level of $[\mathrm{K^+}]$ corresponding to the average value of $[\mathrm{K^+}]$ during HD in the analyzed patients, with the reference T wave (blue) and each investigated T wave (red) being displayed. More peaked T waves with varying width and morphology are observed with increasing $[\mathrm{K^+}]$ levels for the case shown.

C. In Silico Assessment of T wave Changes Due to $[\mathrm{Ca^{2+}}]$ and HR Variations

APs and T wave markers computed from pECGs at varying $[\mathrm{Ca^{2+}}]$ and RR are shown in Fig. 5. Panels (a and b) illustrate changes in APs for simulated case C154 and $\mathcal{F}\{5.4\mathrm{mM}; [\mathrm{Ca^{2+}}]; 1.0\mathrm{s}\}$ under varying $[\mathrm{Ca^{2+}}]$ while panels (e and f) present APs for $\mathcal{F}\{5.4\,\mathrm{mM}; 2.0\mathrm{mM}; \mathrm{RR}\}$ under varying RR for endocardial (black), midmyocardial (green) and epicardial (red) cells of a simulated fiber. Simulated pECGs, and
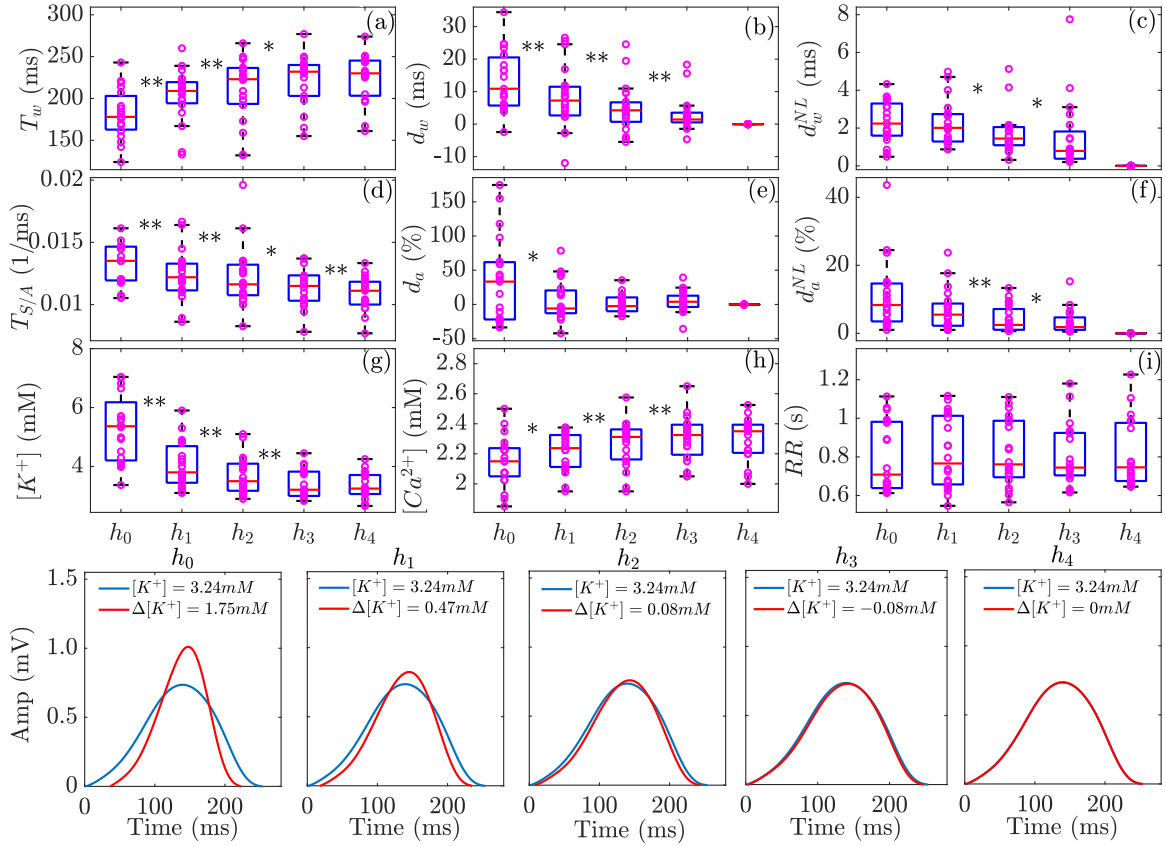
Fig. 3. Panels a–f: Dynamics of T_w, $T_{S/A}$, d_w, d_a, d_w^{NL} and d_a^{NL} during the HD session. Panels g–i: Evolution of $[K^+]$, $[Ca^{2+}]$ and RR during the session. In panels a-i, * indicates $p < 0.05$ and ** indicates $p < 0.01$ in the comparison of each marker between consecutive time points. In each panel, the central line (red) indicates the median, whereas bottom and top edges show the 25th and 75th percentiles, respectively. Each purple dot corresponds to an individual patient. In the bottom panels, red T waves illustrate the PCA-transformed T waves of a patient from the start to the end of the HD session, with $\triangle$ denoting the change in $[K^+]$ with respect to the end of the HD session (h_4). The blue line indicates the reference T wave at the end of the HD session used in the computation of time-warping markers.

specifically T waves, are presented for varying $[Ca^{2+}]$ and RR in panels (c, d, g, h, i and j).

From panels (a-d), it can be observed that lower $[Ca^{2+}]$ causes AP prolongation in all the cell types and, consequently, longer QT intervals. Panel (i) shows that the width and amplitude of the T wave increase with decreasing $[Ca^{2+}]$ and the morphology varies too. From panels (e-h) it can be seen that an increase in the RR interval causes AP prolongation and, thus, longer QT intervals (panels e-h). In the middle panel (j), the width and amplitude of the T wave are shown to increase with increasing RR, which is accompanied by changes in the T wave shape.

Changes in the T wave markers when varying $[Ca^{2+}]$, $\mathcal{F}\{5.4mM; [Ca^{2+}]; 1.0\,s\}$ (red bar), and when varying RR, $\mathcal{F}\{5.4mM; 2.0mM; RR\}$ (green bar), are presented for the 22 simulated cases in panels (k-p) and compared with the changes measured after varying $[K^+]$ $\mathcal{F}\{[K^+]; 2.0mM; 1.0s\}$ (blue bar). A monotonic rise in d_w and d_w^{NL} (panels l and m) as well as decreasing trends in d_a and d_a^{NL} (panels o and p) are observed from the minimum to the maximum levels of $[Ca^{2+}]$. However, T_w and $T_{S/A}$ do not show a clear trend at varying levels of $[Ca^{2+}]$ (panels k and n). As for the effects of increasing RR, trends towards lower $T_{S/A}$, d_w, d_w^{NL} and d_a^{NL} can be observed (panels l,

m, n and p). Similarly, an increasing trend of d_a and a monotonic rise in T_w at increasing RR (panels k and o) are shown.

It can be noted from the figure that T wave markers, particularly morphology-based ones, show remarkable variations at varying $[K^+]$, $[Ca^{2+}]$ and RR. However, $[K^+]$-induced variations are more visible than those induced by $[Ca^{2+}]$ and RR.

D. Contribution of $[K^+]$, $[Ca^{2+}]$ and HR Variations to T Wave Changes in Vivo and in Silico

To assess the relationship between electrolyte or RR variations and the corresponding changes in T wave markers, a correlation analysis was performed, both for ECG recordings from the patients and simulated pECGs. Results are presented in Fig. 6. The three graphics in panel (a) illustrate the linear correlation coefficients ρ between $[K^+]$, $[Ca^{2+}]$ or RR and each of the analyzed T wave markers computed from the patients' ECGs. Panel (b) shows the corresponding linear partial correlation coefficients after removing the effects of the other two covariates ($[K^+]$, $[Ca^{2+}]$ or RR). Panel (c) shows the linear correlation coefficients in the simulated cases at varying $[K^+]$, $[Ca^{2+}]$ and RR.
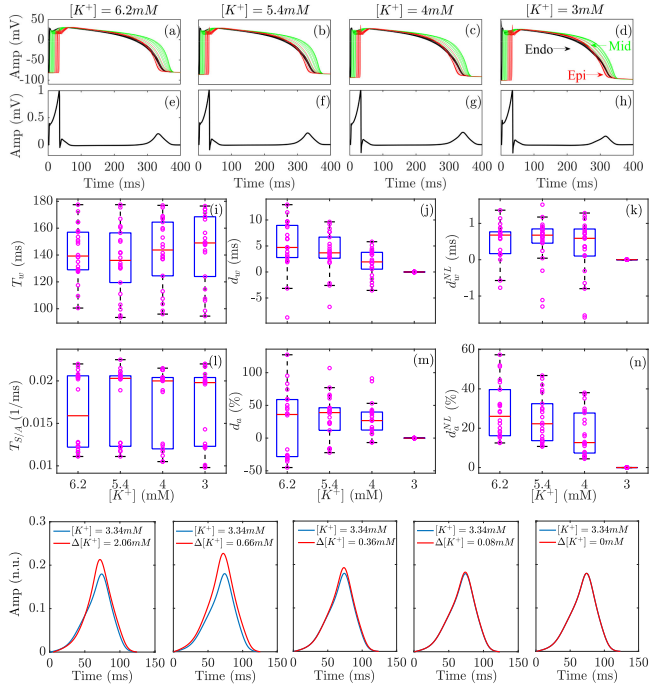
Fig. 4. Panels a-d: Simulated endocardial (black), midmyocardial (green) and epicardial (red) APs for simulated fiber C154, and $\mathcal{F}\{[K^+]; 2.0\,\text{mM}; 1.0\,\text{s}\}$. Panels e-h: ECGs for varying $[K^+]$. Panels i-n: Changes in T_w, $T_{S/A}$, d_w, d_a, d_w^{NL} and d_a^{NL} for simulated fibers when varying $[K^+]$. Central red lines indicate the median, whereas bottom and top edges show the 25th and 75th percentiles, respectively. Each purple dot corresponds to an individual simulated fiber. In the bottom panels, red traces indicate the T waves of a simulated fiber from an initial (maximum) to a final (minimum) value of $[K^+]$ corresponding to average $[K^+]$ values in the analyzed patients. The blue line indicates the reference T wave used when computing time-warping markers.

Fig. 5. Panels a, b: Simulated endocardial (black), midmyocardial (green) and epicardial (red) APs for simulated fiber C154, $\mathcal{F}\{5.4\text{mM}; [Ca^{2+}]; 1.0\,\text{s}\}$ under varying $[Ca^{2+}]$. Panels c, d, i: ECGs and T waves for $[Ca^{2+}]$ variations. Panels e, f: Simulated endocardial (black), midmyocardial (green) and epicardial (red) APs for simulated fiber C154, $\mathcal{F}\{5.4\text{mM}; 2.0\text{mM}; RR\}$, under varying RR. Panels g, h, j: ECGs and T waves for RR variations. Panels k-p: Changes in T_w, $T_{S/A}$, d_w, d_a, d_w^{NL} and d_a^{NL} for varying $[K^+]$, $\mathcal{F}\{[K^+]; 2.0\text{mM}; 1.0\,\text{s}\}$ (blue boxplots), $[Ca^{2+}]$, $\mathcal{F}\{5.4\text{mM}; [Ca^{2+}]; 1.0\,\text{s}\}$ (red boxplots), and RR, $\mathcal{F}\{5.4\text{mM}; 2.0\text{mM}; RR\}$ (green boxplots), in the horizontal axis for the 22 simulated fibers. Central lines indicate the median, whereas bottom and top edges show the 25th and 75th percentiles, respectively. Values of $[K^+] \in \{3.0, 4.0, 5.4, 6.2\}$ mM, $[Ca^{2+}] \in \{1.4, 2.0, 2.6, 3.2\}$ mM, and $RR \in \{0.6, 0.8, 1.0, 1.2\}$ s are used.

Most of the analyzed T wave markers strongly correlated with $[K^+]$. T_w, $T_{S/A}$, d_w and d_a^{NL} were the most highly correlated ones, with median ρ of -0.94, 0.87, 0.88 and 0.80, respectively, in the patients, and -0.97, 0.86, 0.97 and 0.95, respectively, in the simulations. However, only d_a^{NL} was strongly correlated with $[K^+]$ when the effects of $[Ca^{2+}]$ and RR in the patient's data were removed (median value of partial correlation coefficient of 0.75).

Similarly, T_w, $T_{S/A}$, d_w and d_a^{NL} were strongly correlated with $[Ca^{2+}]$ (median value of ρ of 0.79, -0.82, -0.80 and -0.74, respectively, in the patients, and -0.75, 0.91, 0.42 and -0.99, respectively, in the simulations). In this case, only d_w was strongly correlated with $[Ca^{2+}]$ when removing the effects of $[K^+]$ and RR (median value of partial correlation coefficient of -0.74) in the patients' data.

As for the relationship between T wave markers and RR, only d_a presented a strong correlation in both patients' and simulated ECGs (median ρ of -0.67 for Pearson correlation and -0.90 for partial correlation in the patients, and of 0.99 for Pearson correlation in the simulations).

Table II shows the p-values from the Student's t-test applied to assess the statistical significance of non-zero mean Fisher's z-transformed Pearson correlation coefficients between T wave markers and each of $[K^+]$, $[Ca^{2+}]$ and RR in the patient
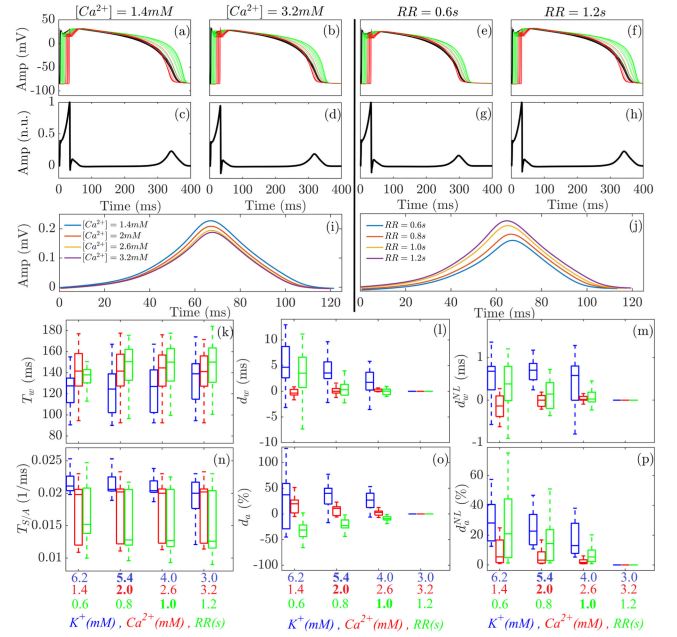
TABLE II
P-VALUES FROM STUDENT'S T-TEST TO EVALUATE STATISTICAL SIGNIFICANCE OF NON-ZERO MEAN FISHER'S Z-TRANSFORMED PEARSON CORRELATION COEFFICIENT BETWEEN T WAVE MARKERS AND EACH OF $[K^+]$, $[Ca^{2+}]$ AND RR IN THE PATIENT POPULATION

p-values	T_w	$T_{S/A}$	d_w	d_a	d_w^{NL}	d_a^{NL}
ρ	ms	1/ms	ms	%	ms	%
$[K^+]$	< 0.01	< 0.01	< 0.01	0.25	< 0.01	< 0.01
$[Ca^{2+}]$	0.03	0.01	0.01	0.73	0.01	< 0.01
RR	0.59	0.79	0.75	0.02	0.98	0.92

population. As can be seen from the table, all the analyzed T wave markers, except for d_a, correlated strongly with $[K^+]$ and $[Ca^{2+}]$. On the other hand, only d_a correlated strongly with RR.

E. Mechanisms for Inter-Individual Differences in the Effects of $[K^+]$, $[Ca^{2+}]$ and RR on T Wave Changes

The results of the linear regression analysis performed to investigate how different proportions of endocardial, midmyocardial and epicardial cells contribute to explain individual T wave responses when varying $[K^+]$ are presented in Fig. 7 for a commonly used T wave marker, T_w, and a morphology-based marker, d_a^{NL}. Cell proportions are represented in the x-axis, with
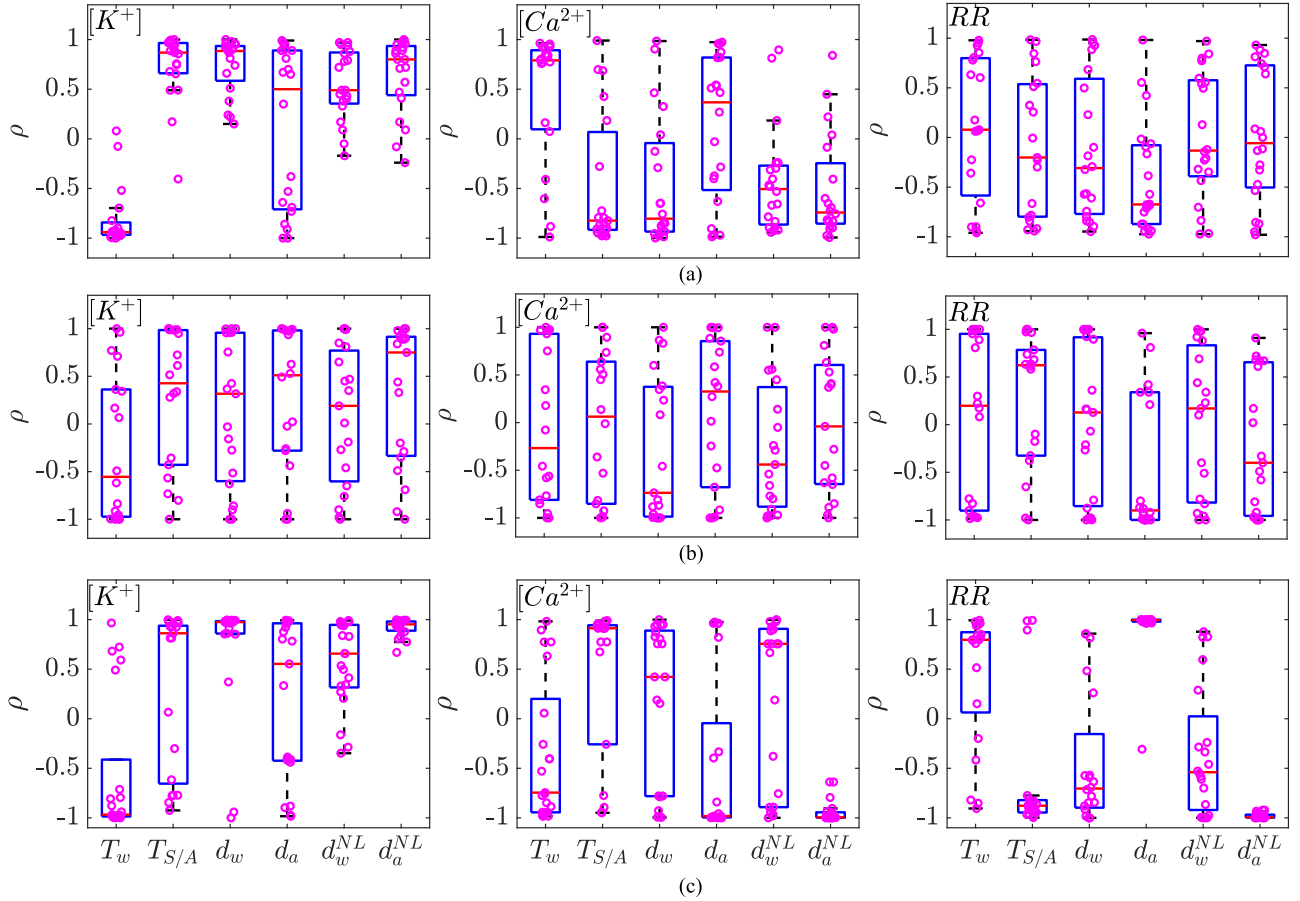
Fig. 6. Panel a: Pearson correlation coefficients between each T wave marker (T_w, $T_\mathrm{S/A}$, d_w, d_a, $d_\mathrm{w}^{\mathrm{NL}}$ and $d_\mathrm{a}^{\mathrm{NL}}$) and $[\mathrm{K}^+]$ (left), $[\mathrm{Ca}^{2+}]$ (middle) or RR (right) for the analyzed patients. Panel b: Partial correlation coefficients between each T wave marker (T_w, $T_\mathrm{S/A}$, d_w, d_a, $d_\mathrm{w}^{\mathrm{NL}}$ and $d_\mathrm{a}^{\mathrm{NL}}$) and $[\mathrm{K}^+]$ (left), $[\mathrm{Ca}^{2+}]$ (middle) or RR (right) for the analyzed patients after removing the effects of the other two variables among $[\mathrm{K}^+]$, $[\mathrm{Ca}^{2+}]$ and RR. Panel c: Pearson correlation coefficients between each T wave marker (T_w, $T_\mathrm{S/A}$, d_w, d_a, $d_\mathrm{w}^{\mathrm{NL}}$ and $d_\mathrm{a}^{\mathrm{NL}}$) and $[\mathrm{K}^+]$ (left), $[\mathrm{Ca}^{2+}]$ (middle) or RR (right) for the simulated fibers under varying $[\mathrm{K}^+]$, $\mathcal{F}\{[\mathrm{K}^+]; 2.0\mathrm{mM}; 1.0\ \mathrm{s}\}$ (left), $[\mathrm{Ca}^{2+}]$, $\mathcal{F}\{5.4\mathrm{mM}; [\mathrm{Ca}^{2+}]; 1.0\ \mathrm{s}\}$ (middle) and RR, $\mathcal{F}\{5.4\mathrm{mM}; 2.0\mathrm{mM}; \mathrm{RR}\}$ (right). Each purple dot represents the correlation coefficient for an individual patient or simulated fiber. Central red lines indicate the median, whereas bottom and top edges show the 25th and 75th percentiles, respectively.

TABLE III
RESULTS OF THE SENSITIVITY ANALYSIS, $S_{Y;c;a_1,a_2}$, FOR DIFFERENT VALUES OF $[\mathrm{K}^+]$, WHEN VARYING CELL PROPORTIONS IN LAYER c FROM a_1 TO a_2

$S_{Y;c;a_1,a_2}$	Y	T_w	$T_\mathrm{S/A}$	d_w	d_a	$d_\mathrm{w}^{\mathrm{NL}}$	$d_\mathrm{a}^{\mathrm{NL}}$
c, a_1, a_2	$[\mathrm{K}^+]$ (mM)	%	%	%	%	%	%
Endo, 10, 50	4.0	2.9	7.2	108.3	21.9	97.7	0.4
	6.2	2.2	7.2	78.7	16.2	3.1	9.7
Mid, 10, 50	4.0	4.5	1.4	41.5	43.5	9.2	10.9
	6.2	0.3	11.1	10.7	53.7	8.2	11.8
Epi, 20, 80	4.0	1.3	8.2	102.3	16.7	86.1	10.1
	6.2	1.1	12.4	41.6	36.8	2.6	17.2

solid lines showing fitted linear regression models for T_w and $d_\mathrm{a}^{\mathrm{NL}}$ for all simulated cases.

Both T_w and $d_\mathrm{a}^{\mathrm{NL}}$ present clear relationships with transmural heterogeneities, being such relationships more or less accentuated depending on the $[\mathrm{K}^+]$ level. The highest sensitivities, shown in Table III, and coefficients of determination, R^2 shown in Fig. 7, of the time-based marker T_w are with respect to

variations in the proportion of endocardial (positive correlation) and midmyocardial cells (negative correlation), with a more notable dependence for low $[\mathrm{K}^+]$ values. In the case of the morphology-based marker $d_\mathrm{a}^{\mathrm{NL}}$, the highest sensitivity and R^2 are observed for midmyocardial (positive correlation) and epicardial (negative correlation) variations, particularly under high $[\mathrm{K}^+]$ values. Sensitivity results for all the analyzed T wave markers at varying $[\mathrm{Ca}^{2+}]$ and RR are presented in Table IV and V.

IV. DISCUSSION

Serum $[\mathrm{K}^+]$ and $[\mathrm{Ca}^{2+}]$ levels outside the normal range are associated with increased mortality [3], [10], [35]–[39]. The availability of non-invasive tools to monitor serum $[\mathrm{K}^+]$ and $[\mathrm{Ca}^{2+}]$ concentrations, particularly in ESRD patients, might have a significant impact on clinical practice. In this work, we characterized changes in ECG markers measuring duration, amplitude and morphology of the T wave during HD in ESRD patients and we assessed their relationship with $[\mathrm{K}^+]$, $[\mathrm{Ca}^{2+}]$
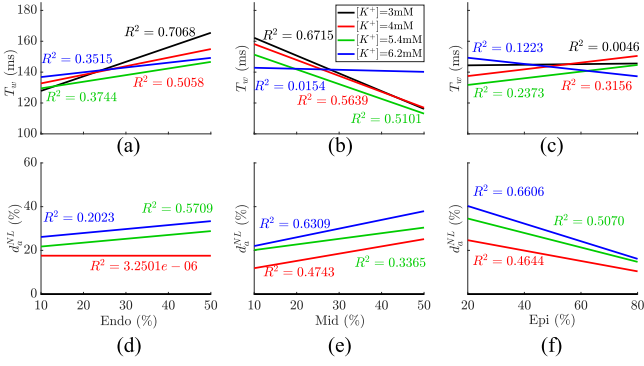
Fig. 7. Panels a-c: Fitted regression lines for the average values of T_{w} for all simulated cases sharing the same proportion of endocardial, midmyocardial or epicardial cells at different $[\mathrm{K}^+]$ levels. Panels d-f: Fitted regression lines for the average values of $d_{\mathrm{a}}^{\mathrm{NL}}$ for all simulated cases sharing the same proportion of endocardial, midmyocardial or epicardial cells at different $[\mathrm{K}^+]$, with the reference value for $[\mathrm{K}^+] = 3$ mM. Coefficients of determination (R^2), estimated as the square of the linear correlation coefficient between the analyzed T wave markers and each cell type (endocardial, midmyocardial or epicardial), are indicated.

TABLE IV

RESULTS OF THE SENSITIVITY ANALYSIS, $S_{Y;c;a_1,a_2}$, FOR DIFFERENT VALUES OF $[\mathrm{Ca}^{2+}]$, WHEN VARYING CELL PROPORTIONS IN LAYER c FROM a_1 TO a_2

$S_{Y;c;a_1,a_2}$	Y	T_{w}	$T_{\mathrm{S/A}}$	d_{w}	d_{a}	$d_{\mathrm{w}}^{\mathrm{NL}}$	$d_{\mathrm{a}}^{\mathrm{NL}}$
c, a_1, a_2	$[\mathrm{Ca}^{2+}]$ (mM)	%	%	%	%	%	%
Endo, 10, 50	1.4	4.5	-11.4	45.0	-22.2	34.2	10.4
	2.6	4.5	-11.6	7.5	-3.9	1.5	10.9
Mid, 10, 50	1.4	0.3	-12.3	39.0	42.3	-11.7	14.1
	2.6	-0.2	-10.4	9.0	63.6	11.2	16.2
Epi, 20, 80	1.4	-0.8	12.7	-84.3	-21.7	-26.5	-19.3
	2.6	0.2	11.1	-14.4	-25.6	-7.0	-25.6

TABLE V

RESULTS OF THE SENSITIVITY ANALYSIS, $S_{Y;c;a_1,a_2}$, FOR DIFFERENT VALUES OF RR, WHEN VARYING CELL PROPORTIONS IN LAYER c FROM a_1 TO a_2

$S_{Y;c;a_1,a_2}$	Y	T_{w}	$T_{\mathrm{S/A}}$	d_{w}	d_{a}	$d_{\mathrm{w}}^{\mathrm{NL}}$	$d_{\mathrm{a}}^{\mathrm{NL}}$
c, a_1, a_2	RR (s)	%	%	%	%	%	%
Endo, 10, 50	0.6	0.5	-0.8	-7.3	-8.4	50.5	4.6
	1.0	0.1	-1.7	-76.7	-11.6	-40.6	-11.1
Mid, 10, 50	0.6	-2.7	-5.2	19.6	32.6	82.2	26.6
	1.0	0.1	-11.3	-29.0	20.6	-1.9	8.7
Epi, 20, 80	0.6	0.3	7.5	-9.3	-16.2	-13.5	-29.9
	1.0	-0.9	12.2	65.7	-7.9	32.6	-14.8

and HR variations. In addition, we simulated human transmural ventricular fibers to unravel potential underpinnings of the high inter-individual differences in T wave responses observed in the patients in response to electrolyte and heart rate variations.

A. T Wave Analysis in ESRD Patients During HD

We evaluated commonly used markers describing T wave time and amplitude characteristics, like its width (T_{w}) and its downward slope-to-amplitude ratio ($T_{\mathrm{S/A}}$), as well as more recently proposed markers describing morphological characteristics computed by warping-based techniques (d_{w}, d_{a}, $d_{\mathrm{w}}^{\mathrm{NL}}$ and $d_{\mathrm{a}}^{\mathrm{NL}}$). Those markers were measured at sequential time

points during HD because large changes in serum electrolyte concentrations can be expected during this period. We showed that such an analysis indeed allows to provide a characterization of T wave changes for a wide range of $[\mathrm{K}^+]$, $[\mathrm{Ca}^{2+}]$ and HR variations, with $d_{\mathrm{a}}^{\mathrm{NL}}$, d_{w} and d_{a} being the markers most strongly correlated with $[\mathrm{K}^+]$, $[\mathrm{Ca}^{2+}]$ and RR, respectively, after removing the effects of the other covariates. These results emphasize the importance of considering more complex markers to fully characterize the ECG repolarization response during HD.

Variations in serum electrolyte levels, mainly $[\mathrm{K}^+]$ and $[\mathrm{Ca}^{2+}]$, have been shown to alter ventricular properties in the ECG [7], [10], [11], [40], [41]. In particular, previous studies have described that ECGs recorded under hyperkalemic conditions commonly have more peaked T waves than those recorded under normal levels of $[\mathrm{K}^+]$ [4], [6], [10], [42]. In this study, we could observe such behavior in some of the ESRD patients' recordings, as illustrated in the bottom panels of Fig. 3. However, a decrease in T wave amplitude could not be consistently measured for all patients, but large inter-individual variability was noted in the relationship between $[\mathrm{K}^+]$ and T wave amplitude. Other studies have analyzed the effects of $[\mathrm{K}^+]$ changes on the width, slope and amplitude-to-slope ratio of the T wave as well as the ratio of the T wave amplitude to the R wave amplitude [14], [15], [17], [43], [44]. The main limitation of these descriptors is that, even if some of them may show a high degree of correlation with the level of $[\mathrm{K}^+]$, their changes cannot be exclusively attributed to $[\mathrm{K}^+]$ variations, as confirmed in our study by including in the analysis additional confounders like variations in $[\mathrm{Ca}^{2+}]$ or HR.

Regarding the analysis of the T wave shape, a morphology combination score (MCS) based on T wave asymmetry, flatness and notching [45]–[47] has been used to analyze its relationship with $[\mathrm{K}^+]$ in a primary care population [48]. A clear association between MCS and $[\mathrm{K}^+]$ could only be found among individuals with $[\mathrm{K}^+]$ in the range 2–4.1 mM, but not among those with $[\mathrm{K}^+]$ in the range 4.2–6 mM. In ESRD patients, we found that morphological variability, specifically quantified by our analyzed T wave marker $d_{\mathrm{a}}^{\mathrm{NL}}$ was closely related to serum $[\mathrm{K}^+]$ in a wide range of values, covering both hyper- and hypokalemic values.

As for the effects of $[\mathrm{Ca}^{2+}]$ variations on the ECG, a recent large-scale study has found that low $[\mathrm{Ca}^{2+}]$ values are associated with clinically relevant QT prolongation in the general population [7]. In chronic patients undergoing HD, changes in $[\mathrm{Ca}^{2+}]$ have been found to be negatively correlated with changes in the last part of the ECG repolarization measured by the T-peak to T-end interval [49]. In this study, we showed that the full repolarization duration measured by T_{w} indeed presents an inverse relationship with $[\mathrm{Ca}^{2+}]$ after removing the effects of other confounders. Nevertheless, such a relationship between T_{w} and $[\mathrm{Ca}^{2+}]$ was not as strong as that of other markers like d_{w} reflecting temporal variations in T wave morphology.

B. T Wave Analysis in Simulated Ventricular Tissues At Varying $[\mathrm{K}^+]$, $[\mathrm{Ca}^{2+}]$ and HR

All the T wave markers analyzed in this study showed a diversity of patterns in their relationship with electrolyte variations

during HD. Both the general trend of such relationships and the high inter-individual variability were well reproduced by our simulated ventricular fibers for most of the markers. This can be explained by the fact that we simulated 22 different transmural fibers accounting for proportions of endocardial, midmyocardial and epicardial cells varying within plausible limits, as reported in previous studies [29], [34], [50], [51]. We are not aware of other *in silico* studies investigating morphological variability in the T wave of the ECG in relation to electrolyte variations such as those occurring during HD, but there are different *in silico* studies characterizing T wave duration and amplitude as a function of electrolyte concentrations [15], [16].

In agreement with our ECG data, an increase in $[K^+]$ led to shortening of the repolarization time quantified by T_w in our transmural fibers. Other computational studies have shown divergent results in this regard. In [18], prolongation of the RT interval has been reported in response to increased $[K^+]$, which is acknowledged by the authors to be in contrast with clinical data but possibly explained by factors other than $[K^+]$. In [15], [52], a simulated increase in $[K^+]$ has been shown to lead to QT shortening, which would be in line with our results. Our results on T_w reduction with increasing $[Ca^{2+}]$ are concordant with the shortening of the repolarization time reported by others [16], [50], [52]. Also, our results at the cellular level are aligned with those obtained with the human ventricular AP model recently proposed by Bartolucci *et al.* [53], which, in contrast to most AP models, is able to reproduce a physiological APD-$[Ca^{2+}]$ relationship.

Moreover, in our simulations, the marker $T_{S/A}$ quantifying the T wave slope-to-amplitude ratio was shown to correlate strongly with $[K^+]$ and $[Ca^{2+}]$. These results are in agreement with previous studies [14], [15], in which $T_{S/A}$ was proposed as an index to monitor $[K^+]$ during HD and a cause-effect sequence for the observed decrease in $T_{S/A}$ was provided through computational simulations.

The above discussed results show that *in silico* modeling and simulation can help to gain insight into the ECG changes observed in response to electrolyte abnormalities. In contrast to other computational studies, which used one single cell or tissue electrophysiological model, we simulated a population of human ventricular tissue fibers, which can be used to shed light on the highly inter-individual relationships between ECG markers and $[K^+]$ or $[Ca^{2+}]$.

C. Potential Mechanisms for Inter-Individual T Wave Responses to Electrolyte and HR Variations

We computed T wave marker sensitivities to explain how different transmural heterogeneities can contribute to explain distinct T wave responses to variations in $[K^+]$, $[Ca^{2+}]$ and HR. The morphological descriptors d_w, d_w^{NL}, d_a and d_a^{NL} generally showed higher sensitivity to variations in the proportions of the ventricular layers than the time and amplitude markers T_w and $T_{S/A}$. Previous experimental and theoretical studies have described how cell distributions across the ventricular wall affect ECG repolarization and, in particular, T wave morphology [22], [54]–[59]. Our study confirms these observations on the impact

of transmural heterogeneities on T wave width, amplitude and shape characteristics, not only at physiological electrolyte concentrations but also at high and low $[K^+]$ and $[Ca^{2+}]$ levels and at different heart rates. Even if transmural heterogeneities can contribute to inter-individual differences in the T wave response to electrolyte and HR variations, other ventricular heterogeneities, like interventricular, apicobasal or anteroposterior, may play a relevant role, which should be assessed in further studies.

Our results on the sensitivity of T wave morphological markers with respect to variations in transmural heterogeneities, and more specifically to the proportion of epicardial cells within the ventricular wall, are aligned with computational findings presented by Janusek *et al.* [54], which demonstrated the influence of epicardial cells on the development of T wave alternans, a form of repolarization variability [54]. The contribution of variations in the midmyocardial layer to T wave morphology has been shown in a recent study too [56].

D. Study Limitations and Future Research

This study investigated 20 ECG recordings of ESRD patients during an HD session, with 5 blood samples available along HD. Future studies should investigate application of the proposed methods to larger numbers of patients and, if possible, with more available blood samples during the full 48-hour ECG recording. This would allow more robust assessment of the relationship between changes in T wave markers and specific variations in $[K^+]$, $[Ca^{2+}]$ or HR, potentially using nonlinear regression statistical techniques [60], [61].

Other electrolytes on top of $[K^+]$ and $[Ca^{2+}]$ could modulate T wave changes during HD. In particular, variations in magnesium ($[Mg^{2+}]$) have been reported to be possibly involved in observed alterations in ECG repolarization [7], [62]–[64]. In the present study, $[Mg^{2+}]$ was not investigated due to the unavailability of serum $[Mg^{2+}]$ levels.

Our electrophysiological simulations considered human transmural ventricular fibers. Future research is aimed at extending the investigations of the present study to include simulations in bi-ventricular models embedded in patient-specific torso models, from which more realistic ECGs can be computed. This research will additionally allow exploring the role of other types of ventricular heterogeneities, on top of transmural ones, on the T wave response to electrolyte and HR variations.

V. CONCLUSION

Descriptors of T wave width (T_w), slope-to-amplitude ratio ($T_{S/A}$) and morphological variability (d_w, d_a, d_w^{NL} and d_a^{NL}) vary remarkably with varying $[K^+]$, $[Ca^{2+}]$ and HR, but a wide range of patterns is observed for such relationships. Among the proposed descriptors, d_a^{NL} d_w and d_a are the ones that best correlate with $[K^+]$, $[Ca^{2+}]$ and HR, respectively. The proportion of midmyocardial and epicardial cells has a large impact on T wave markers, particularly for serum electrolyte concentrations and HR out of their physiological levels. This suggests that transmural heterogeneities can modulate patient-dependent T wave responses to changes in electrolyte concentrations and HR in ESRD patients. These findings can have major relevance

for non-invasive monitoring and prediction of arrhythmic events in these patients.

ACKNOWLEDGMENT

REFERENCES

[1] N. R. Hill *et al.*, "Global prevalence of chronic kidney disease – A systematic review and meta-analysis," *PloS One*, vol. 11, no. 7, 2016, p. e0158765.

[2] M. Kanbay *et al.*, "Sudden death in hemodialysis: An update," *Blood Purification*, vol. 30, no. 2, pp. 135–145, 2010.

[3] H. Bozbas *et al.*, "Prevalence and predictors of arrhythmia in end stage renal disease patients on hemodialysis," *Renal Failure*, vol. 29, no. 3, pp. 331–339, Jan. 2007.

[4] J. N. Weiss *et al.*, "Electrophysiology of hypokalemia and hyperkalemia," *Circulation. Arrhythmia Electrophysiol.*, vol. 10, no. 3, 2017.

[5] J. Soar *et al.*, "European resuscitation council guidelines for resuscitation 2010 Section 8. cardiac arrest in special circumstances: Electrolyte abnormalities, poisoning, drowning, accidental hypothermia, hyperthermia, asthma, anaphylaxis, cardiac surgery, trauma, pregnancy, electrocution," *Resuscitation*, vol. 81, no. 10, pp. 1400–1433, Oct. 2010.

[6] J. T. Levis, "ECG diagnosis: hypokalemia," *Permanente J.*, vol. 16, no. 2, p. 57, 2012.

[7] R. Noordam *et al.*, "Effects of calcium, magnesium, and potassium concentrations on ventricular repolarization in unselected individuals," *J. Amer. College Cardiol.*, vol. 73, no. 24, pp. 3118–3131, Jun. 2019.

[8] D. Poulikakos *et al.*, "Risk of sudden cardiac death in chronic kidney disease," *J. Cardiovasc. Electrophysiol.*, vol. 25, no. 2, pp. 222–231, 2014.

[9] A. Lanari *et al.*, "Electrocardiographic effects of potassium. I. Perfusion through the coronary bed," *Amer. Heart J.*, vol. 67, no. 3, pp. 357–363, Mar. 1964.

[10] N. El-Sherif and G. Turitto, "Electrolyte disorders and arrhythmogenesis," *Cardiol. J.*, vol. 18, no. 3, pp. 233–245, 2011.

[11] C. Van Mieghem *et al.*, "The clinical value of the ECG in noncardiac conditions," *Chest*, vol. 125, no. 4, pp. 1561–1576, Apr. 2004.

[12] Z. I. Attia *et al.*, "Novel bloodless potassium determination using a signal-processed single-lead ECG," *J. Amer. Heart Assoc.: Cardiovasc. Cerebrovascular Dis.*, vol. 5, no. 1, Jan. 2016.

[13] S. Severi *et al.*, "Noninvasive potassium measurements from ECG analysis during hemodialysis sessions," in *Proc. 36th Annu. Cardiol. Conf.*, Sep. 2009, pp. 821–824.

[14] C. Corsi *et al.*, "Validation of a novel method for non-invasive blood potassium quantification from the ECG," in *Proc. Comput. Cardiol.*, Sep. 2012, pp. 105–108.

[15] C. Corsi *et al.*, "Noninvasive quantification of blood potassium concentration from ECG in hemodialysis patients," *Sci. Rep.*, vol. 7, 2017, Art. no. 42492.

[16] M. Hernández Mesa *et al.*, "Effects of serum calcium changes on the cardiac action potential and the ECG in a computational model," *Current Directions Biomed. Eng.*, vol. 4, no. 1, pp. 251–254, Sep. 2018.

[17] S. Kharche *et al.*, "Simulating the effects of serum potassium on the ECG," in *Proc. Comput. Cardiol.*, Sep. 2012, pp. 225–228.

[18] N. Pilia *et al.*, "ECG as a tool to estimate potassium and calcium concentrations in the extracellular space," in *Comput. Cardiol.*, Sep. 2017, pp. 1–4.

[19] H. A. Bukhari *et al.*, "Transmural ventricular heterogeneities play a major role in determining T-wave morphology at different extracellular potassium levels," in *Comput. Cardiol.*, Sep. 2019, pp. 1–4.

[20] J. P. Martínez *et al.*, "A wavelet-based ECG delineator: Evaluation on standard databases," *IEEE Trans. Bio-Med. Eng.*, vol. 51, no. 4, pp. 570–581, Apr. 2004.

[21] F. Castells *et al.*, "Principal component analysis in ECG signal processing," *EURASIP J. Adv. Signal Process.*, vol. 2007, no. 1, pp. 1–21, Dec. 2007.

[22] J. Ramírez *et al.*, "Variability of ventricular repolarization dispersion quantified by time-warping the morphology of the T-waves," *IEEE Trans. Bio-Med. Eng.*, vol. 64, no. 7, pp. 1619–1630, Jul. 2017.

[23] D. Freedman *et al.*, "Statistics," 4th ed., WW Norton & Company, New York, 2007.

[24] J. Benesty *et al.*, "Pearson correlation coefficient," in *Noise Reduction in Speech Processing*. Springer, 2009, pp. 37–40.

[25] Y. Zuo *et al.*, "Biological network inference using low order partial correlation," *Methods*, vol. 69, no. 3, pp. 266–273, Oct. 2014.

[26] J. L. Fleiss and J. M. Tanur, "A note on the partial correlation coefficient," *Amer. Statistician*, vol. 25, no. 1, pp. 43–45.

[27] J. D. Gibbons and S. Chakraborti, "Nonparametric statistical inference," in *Int. Encyclopedia Stat. Sci.*, M. Lovric, Ed. Berlin, Heidelberg: Springer Berlin Heidelberg, 2011, pp. 977–979.

[28] R. A. Fisher, "Statistical methods for research workers," in *Breakthroughs in Statistics: Methodology and Distribution*, ser. Springer Series in Statistics, S. Kotz and N. L. Johnson, Eds. New York, NY: Springer, 1992, pp. 66–70.

[29] K. Gima and Y. Rudy, "Ionic current basis of electrocardiographic waveforms: A model study," *Circulation Res.*, vol. 90, no. 8, pp. 889–896, May 2002.

[30] K. H. W. J. Ten Tusscher and A. V. Panfilov, "Alternans and spiral breakup in a human ventricular tissue model," *Amer. J. Physiol.-Heart Circulatory Physiol.*, vol. 291, no. 3, pp. H1088–H1100, Sep. 2006.

[31] S. Severi *et al.*, "From in vivo plasma composition to in vitro cardiac electrophysiology and in silico virtual heart: The extracellular calcium enigma," *Philos. Trans. Ser. A, Math., Phys., Eng. Sci.*, vol. 367, no. 1896, pp. 2203–2223, Jun. 2009.

[32] E. A. Heidenreich *et al.*, "Adaptive macro finite elements for the numerical solution of monodomain equations in cardiac electrophysiology," *Ann. Biomed. Eng.*, vol. 38, no. 7, pp. 2331–2345, Jul. 2010.

[33] L. Romero *et al.*, "Impact of ionic current variability on human ventricular cellular electrophysiology," *Amer. J. Physiol. Heart Circulatory Physiol.*, vol. 297, no. 4, pp. H1436–1445, Oct. 2009.

[34] E. Pueyo *et al.*, "Mechanisms of ventricular rate adaptation as a predictor of arrhythmic risk," *Amer. J. Physiol.-Heart Circulatory Physiol.*, vol. 298, no. 5, pp. H1577–H1587, Mar. 2010.

[35] J. H. Brown *et al.*, "Comparative mortality from cardiovascular disease in patients with chronic renal failure," *Nephrol., Dialysis, Transplant.: Official Pub. Eur. Dialysis Transplant. Assoc. - Eur. Renal Assoc.*, vol. 9, no. 8, pp. 1136–1142, 1994.

[36] M. L. Krogager *et al.*, "Short-term mortality risk of serum potassium levels in hypertension: a retrospective analysis of nationwide registry data," *Eur. Heart J.*, vol. 38, no. 2, pp. 104–112, 2017.

[37] B. Pitt and P. Rossignol, "The association between serum potassium and mortality in patients with hypertension: 'A wake-up call'," *Eur. Heart J.*, vol. 38, no. 2, pp. 113–115, 2017.

[38] A. Loewe *et al.*, "Sinus bradycardia due to electrolyte changes as a potential pathomechanism of sudden cardiac death in hemodialysis patients," *Biophy. J.*, vol. 116, no. 3, p. 231a, Feb. 2019.

[39] F. Ajam, "Cardiac arrhythmias in patients with end stage renal disease (ESRD) on hemodialysis; recent update and brief literature review," *Amer. J. Internal Med.*, vol. 7, no. 1, pp. 22–26, 2019.

[40] J. D. Gardner *et al.*, "ECG diagnosis: the effect of ionized serum calcium levels on electrocardiogram," *Permanente J.*, vol. 18, no. 1, pp. e119–e120, 2014.

[41] E. Chorin *et al.*, "Electrocardiographic manifestations of calcium abnormalities," *Ann. Noninvasive Electrocardiol. : Official J. Int. Soc. Holter Noninvasive Electrocardiol., Inc*, vol. 21, no. 1, pp. 7–9, Nov. 2015.

[42] C. Slovis and R. Jenkins, "ABC of clinical electrocardiography: Conditions not primarily affecting the heart," *BMJ (Clinical Research ed.)*, vol. 324, no. 7349, pp. 1320–1323, Jun. 2002.

[43] J. J. Dillon *et al.*, "Noninvasive potassium determination using a mathematically processed ECG: Proof of concept for a novel "bloodless, blood test"," *J. Electrocardiol.*, vol. 48, no. 1, pp. 12–18, Feb. 2015.

[44] P. Frohnert Peter *et al.*, "Statistical investigation of correlations between serum potassium levels and electrocardiographic findings in patients on intermittent hemodialysis therapy," *Circulation*, vol. 41, no. 4, pp. 667–676, Apr. 1970.

[45] M. Andersen *et al.*, "A robust method for quantification of IKr-related T-wave morphology abnormalities," *Comput. Cardiol.*, Sep. 2007, pp. 341–344.

[46] L. Hong *et al.*, "T-wave morphology analysis of competitive athletes," *J. Electrocardiol.*, vol. 48, no. 1, pp. 35–42, Feb. 2015.

[47] S. G. Tischer *et al.*, "Influence of type of sport on cardiac repolarization assessed by electrocardiographic T-wave morphology combination score," *J. Electrocardiol.*, vol. 51, no. 2, pp. 296–302, Mar. 2018.

[48] M. L. Krogager *et al.*, "The relationship between serum potassium concentrations and electrocardiographic characteristics in 163,547 individuals from primary care," *J. Electrocardiol.*, vol. 57, pp. 104–111, Dec. 2019.

[49] H. Ozportakal *et al.*, "Hemodialysis-induced repolarization abnormalities on ECG are influenced by serum calcium levels and ultrafiltration volumes," *Int. Urol. Nephrol.*, vol. 49, no. 3, pp. 509–515, Mar. 2017.

[50] A. Loewe *et al.*, "A heterogeneous formulation of the Himeno et al human ventricular myocyte model for simulation of body surface ECGs," in *Proc. Comput. Cardiol. Conf.*, Sep. 2018, vol. 45, pp. 1–4.

[51] E. Pueyo *et al.*, "A multiscale investigation of repolarization variability and its role in cardiac arrhythmogenesis," *Biophy. J.*, vol. 101, no. 12, pp. 2892–2902, Dec. 2011.

[52] N. Pilia *et al.*, "ECG-based estimation of potassium and calcium concentrations: Proof of concept with simulated data," in *Proc. 41st Annu. Int. Conf.IEEE Eng. Med. Biol. Soc.*, Jul. 2019, pp. 2610–2613.

[53] C. Bartolucci *et al.*, "Simulation of the effects of extracellular calcium changes leads to a novel computational model of human ventricular action potential with a revised calcium handling," *Front. Physiol.*, vol. 11, Apr. 2020.

[54] D. Janusek *et al.*, "The roles of mid-myocardial and epicardial cells in T-wave alternans development: A simulation study," *Biomed. Eng. Online*, vol. 17, no. 1, p. 57, May 2018.

[55] M. W. Rivolta *et al.*, "T-wave morphology depends on transmural heterogeneity in a high-resolution human left-ventricular wedge model," in *Proc. Comput. Cardiol. Conf.*, Sep. 2015, pp. 433–436.

[56] P. K. Priya and S. Jayaraman, "Do M-cells contribute significantly in T-wave morphology during normal and arrhythmogenesis conditions like short QT Syndrome?," *bioRxiv*, May 2020, Art. no. 121079.

[57] J.-I. Okada *et al.*, "Transmural and apicobasal gradients in repolarization contribute to T-wave genesis in human surface ECG," *Amer. J. Phys. Heart Circulatory Physiol.*, vol. 301, no. 1, pp. H200–208, Jul. 2011.

[58] N. T. Srinivasan *et al.*, "Differences in the upslope of the precordial body surface ECG T wave reflect right to left dispersion of repolarization in the intact human heart," *Heart Rhythm*, vol. 16, no. 6, pp. 943–951, 2019.

[59] B. Hooft van Huysduynen *et al.*, "Validation of ECG indices of ventricular repolarization heterogeneity: A computer simulation study," *J. Cardiovasc. Electrophysiol.*, vol. 16, no. 10, pp. 1097–1103, Oct. 2005.

[60] A. J. Izenman, "*Modern Multivariate Statistical Techniques: Regression, Classification, and Manifold Learning*," Springer texts in statistics, New York, 2008.

[61] N. R. Draper and H. Smith, *Applied Regression Analysis*, 3rd ed., ser. Wiley series in probability and statistics. New York: Wiley, 1998.

[62] N. Naksuk *et al.*, "Association of serum magnesium on mortality in patients admitted to the intensive cardiac care unit," *Amer. J. Med.*, vol. 130, no. 2, pp. 229.e5–229.e13, Feb. 2017.

[63] W. K. Jhang *et al.*, "Severe hypermagnesemia presenting with abnormal electrocardiographic findings similar to those of hyperkalemia in a child undergoing peritoneal dialysis," *Korean J. Pediatrics*, vol. 56, no. 7, pp. 308–311, Jul. 2013.

[64] W. M. van den Bergh *et al.*, "Electrocardiographic abnormalities and serum magnesium in patients with subarachnoid hemorrhage," *Stroke*, vol. 35, no. 3, pp. 644–648, Mar. 2004.